

A cross-bispectrum estimator for CMB-HI intensity mapping correlations

Kavilan Moodley^{1,2,*}, Warren Naidoo¹, Heather Prince^{1,3,4}, and Aurelie Penin¹

¹ *Astrophysics Research Centre & School of Mathematics, Statistics and Computer Science,
University of KwaZulu-Natal, Durban, 4041, South Africa*

² *Center for Computational Astrophysics, Flatiron Institute, 162 5th Avenue, 10010, New York, NY, USA*

³ *Department of Astrophysical Sciences, Peyton Hall,
Princeton University, Princeton, NJ 08544, USA and*

⁴ *Department of Physics and Astronomy, Rutgers, The State University of New Jersey,
136 Frelinghuysen Rd, Piscataway, NJ 08854, USA*

(Dated: November 13, 2023)

Intensity mapping of 21cm emission from neutral hydrogen (HI) promises to be a powerful probe of large-scale structure in the post-reionisation epoch. However, HI intensity mapping (IM) experiments will suffer the loss of long-wavelength line-of-sight HI modes in the galactic foreground subtraction process. The loss of these modes is particularly problematic for HI IM cross-correlations with projected large-scale structure tracers, such as CMB secondary anisotropies, with the constraining power of the cross-correlation power spectrum being significantly reduced by this mode loss. Here we propose a cross-bispectrum estimator to recover the cross-correlation of the HI IM field, δT_{21} , with the CMB lensing field, κ , constructed by correlating the position-dependent HI power spectrum with the mean overdensity traced by CMB lensing.

We study the cross-bispectrum estimator, $B^{\kappa\delta T_{21}\delta T_{21}}$, in the squeezed limit and forecast its detectability based on HI IM measurements from the Hydrogen Intensity mapping and Realtime Analysis eXperiment (HIRAX) and CMB lensing measurements from the Atacama Cosmology Telescope (Advanced ACT). When the HI-CMB lensing cross-bispectrum is combined with the HI IM and CMB lensing auto-power spectra, the *combined* constraint on the HI-density weighted growth rate of fluctuations, $f\Omega_{HI}$, is at the sub-percent level, independent of the small-scale amplitude of fluctuations, σ_8 , which is constrained at the 0.02% level. The degeneracy between these two parameters is broken by the cross-bispectrum and HI power spectrum probing different combinations of these parameters.

The cross-bispectrum improves constraints on cosmological parameters; in particular, the constraint on the dark energy equation-of-state parameter, w_0 , improves on the HI IM auto-power spectra constraint by 44% (to 0.014), while the constraint on w_a improves by 33% (to 0.08), assuming Planck priors in each case. Even when varying the spatial curvature, we find that the constraint on w_0 improves on the HI IM auto-power spectra constraint by 29% (to 0.022) while the constraint on w_a improves by 31% (to 0.09). These results are robust to HI IM foreground removal because they largely derive from small-scale HI modes. The HI-HI- κ cross-bispectrum thus provides a novel way to recover HI correlations with CMB lensing and constrain cosmological parameters at a level that is competitive with next-generation galaxy redshift surveys. As a striking example of this, we find that the *combined* constraint on the sum of the neutrino masses, while varying all redshift and standard cosmological parameters within a $w_0w_a\Omega_K$ CDM model, is 5.5 meV.

PACS numbers:

INTRODUCTION

Intensity mapping of the cosmic microwave background has provided exquisite measurements of linear cosmological modes projected along the line of sight, thereby enabling the most precise constraints on the cosmological model to date [1–4]. Going beyond these constraints will require probes of the three-dimensional large-scale structure that measure this much larger set of cosmological modes to high precision. Galaxy redshift surveys [5–7] and post-reionisation hydrogen intensity mapping experiments [8–14] targeting the baryon acoustic oscillation (BAO) signal as a probe of dark energy [15–17], will map the large-scale structure distribution out to high redshift and over large survey areas, thereby expanding our access to three-dimensional cosmological

modes.

Intensity mapping surveys of the 21cm hydrogen line [15, 18] promise to be a relatively efficient probe for mapping large-scale structure using a single tracer over a large redshift range and large sky area; HI redshifts are measured simultaneously when imaging unlike optical and infrared tracers, HI is ubiquitous in the universe out to the redshift of reionisation, and in the case of dish interferometer experiments the survey speed benefits from both a large number of relatively inexpensive dishes, scaling as the square of the collecting area, and the low-resolution of the compact array that has a wider field-of-view and excellent brightness sensitivity to large scales [19].

HI intensity mapping experiments face unique challenges, though. The galactic synchrotron and extragalactic point source signals are several orders of magnitude larger than the cosmological HI signal [20]. The proposed

solution to this is to take advantage of the smooth power law frequency spectra of these contaminants by high-pass filtering the data in the frequency domain [16, 21], leaving behind the HI signal that is correlated in frequency over smaller separations, corresponding to the BAO scale along the line of sight. However, imperfect data calibration from a strongly chromatic interferometer threatens to leak power from smooth line-of-sight foreground modes into higher frequency HI modes [22, 23] so the focus in the field has primarily been on overcoming these systematic effects.

These challenges have meant that the HI intensity mapping signal has not yet been detected in auto-correlation (though see [24] for a recently reported detection on small-scales). However, we know the signal is present as it has been detected in cross-correlation with spectroscopic galaxy surveys [25–28]. Going beyond the current HI cross-correlation detections, the astrophysical and cosmological constraints that could be provided by future HI cross-correlations has been studied in the literature [29–32]. These studies have utilised the simplest 2-point cross-correlation statistics of HI with either galaxy, cosmic shear or CMB lensing surveys.

Cross-correlations of HI intensity mapping with CMB secondary anisotropies are interesting because of the unique physics, either gravitational or scattering, imprinted on the CMB by large-scale structure [33–36]. However, due to the absence of large-scale line-of-sight modes in the HI signal as a result of foreground filtering, the cross-power spectrum between HI intensity mapping and the CMB is significantly reduced, as we argue in this letter. The loss of cross-correlation signal with HI is also relevant, to an extent, for photometric galaxy surveys, which have relatively broad redshift bins compared to spectroscopic redshift surveys. To recover the correlation between HI intensity mapping and CMB secondary anisotropies, we propose the use of a higher-order correlation that takes advantage of the modulation of small-scale HI modes by a large-scale density mode. An alternative, but related, approach is to reconstruct the long wavelength density modes using the small-scale HI modes and then correlate this field with the projected CMB field [37–39]. In this letter, we specifically present a HI-CMB lensing cross-bispectrum estimator that comprises two HI fields, which have well-measured small-scale modes, and a CMB lensing convergence field, and study the constraining power of this cross-bispectrum in combination with the corresponding auto-power spectra.

The rest of this paper is structured as follows. In section 1, we discuss why the HI-CMB lensing cross-spectrum vanishes. In section 2, we present the HI-CMB lensing cross-bispectrum estimator. Finally, in section 3, we study cosmological parameter constraints from the HI-CMB lensing cross-bispectrum using the Fisher matrix. In our analysis, we assume the Planck 2018 cosmology and priors [40]: $h = 0.67$, $\Omega_M = 0.315$, $\Omega_\Lambda = 0.684$,

$\Omega_k = 0.0$, $n_s = 0.965$, $\sigma_8 = 0.811$, $w_0 = -1.03$ and $N_{eff} = 2.99$. All distances and scales are expressed in physical (Mpc), rather than h^{-1} Mpc, units.

WHY THE TWO-POINT CORRELATION OF HI INTENSITY AND A CMB SECONDARY SIGNAL IS NEGLIGIBLE

We show here that the cross-correlation between a projected CMB secondary signal, which has a broad redshift kernel, and an HI intensity map, which has been cleaned of foregrounds and thus lacking long-wavelength radial modes, is negligible due to the lack of overlap in large-scale radial modes. Specifically, we consider the cross-correlation between the HI intensity mapping signal and the CMB lensing convergence signal in a periodic comoving volume, $V_p(z_i) = \chi_i^2 r_{\nu,i}$, spanning a redshift slice centred at redshift z_i , with width Δz (~ 0.5) corresponding to a dimensionless bandwidth, $\Delta\tilde{\nu}_i$, and subtending a solid angle, Ω_i , on the sky. Working in this “snapshot” geometry [15, 41] we have χ_i and $r_{\nu,i} = \chi_i/\tilde{\nu}_i$ (where $\tilde{\nu}_i = \nu_i/\nu_{21}$) defining the transverse and line-of-sight comoving distances, which project physical wavenumbers within the volume to angular and radial wavenumbers as $\mathbf{k}_\perp = \ell/\chi_i$ and $k_\parallel = y/r_{\nu,i}$, respectively.

The angular HI signal in this volume is given by [15]

$$\delta T_{21}(\ell, y; z_i) = \bar{T}_b(z_i) Z_{HI}(\mathbf{k}; z_i) \delta_m(\mathbf{k}, z_i)/V_p(z_i),$$

where \bar{T}_b is the mean brightness temperature, $Z_{HI}(\mathbf{k}; z_i) = b_{HI}^{(1)}(z_i) + f(z_i)\mu_k^2$ includes the linear bias and redshift space distortion terms that relate the HI density field to the underlying matter density field, δ_m . The HI signal is swamped by galactic and extragalactic foregrounds [20] though these can be filtered out by taking advantage of the smooth frequency dependence of the foregrounds [22, 42] to recover the HI signal. However, the consequence of foreground filtering is that low k_\parallel modes in the HI signal are removed, typically below a wavenumber $k_\parallel \sim 0.01$ Mpc $^{-1}$ [15].

The CMB lensing convergence, $\kappa(\boldsymbol{\theta}) = \int d\chi \kappa(\mathbf{r})$, is the projection of the matter density along the line-of-sight [43], where $\kappa(\mathbf{r}) = W_\kappa(\chi)\delta_m(\mathbf{r})$ is given in terms of the lensing convergence redshift kernel, $W_\kappa(\chi) = \frac{3}{2}\Omega_{m0}(H_0\chi/c)^2(1+z)\left(\frac{\chi_*-\chi}{\chi_*\chi}\right)$, and χ_* is the comoving distance to the last scattering surface. We will find it convenient to define the lensing contribution within the redshift bin z_i as $\kappa(\boldsymbol{\theta}; z_i) = \int d\chi \kappa(\mathbf{r}; z_i)$.

In harmonic space, the lensing convergence is given by

$$\kappa(\ell) = \int \frac{dk_\parallel}{(2\pi)} \int d\chi e^{ik_\parallel\chi} K_\kappa(\chi) \frac{\delta_m(\ell/\chi, k_\parallel, z=0)}{\chi^2},$$

where $K_\kappa(\chi) = D(\chi)W_\kappa(\chi)$ and D is the growth function. The CMB lensing kernel has broad redshift support between today and last scattering, which means that

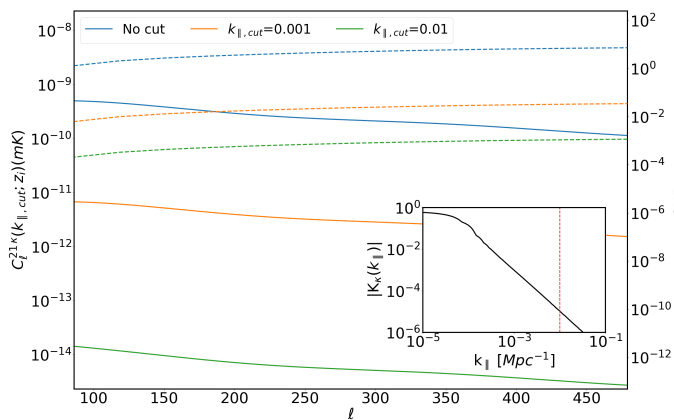


FIG. 1: Hi -CMB lensing cross-correlation signal (solid lines) as a function of angular wavenumber for three different values of $k_{||,cut}$ computed in the $z_i = 1.27$ redshift bin. The corresponding dashed lines show the signal-to-noise ratio (SNR) for each case. In the inset plot, we show the CMB lensing kernel in Fourier space, which rapidly falls off with increasing $k_{||}$, and the nominal value of $k_{||,cut}$ that we use in this paper.

most of the lensing signal is contained in low $k_{||} \sim \chi_*^{-1}$ modes, as shown in the Figure 1 inset.

Note that our description of the CMB lensing signal in terms of $k_{||}$ modes is approximate, due to evolution within the broad redshift bin. However, $\tilde{K}_{\kappa}(k_{||})$, the radial transform of $K_{\kappa}(\chi)$, is only used here for conceptual value and a more precise treatment would require a light-cone decomposition into suitable angular and radial modes.

The lensing convergence and HI IM cross-correlation spectrum in redshift bin z_i is given by

$$C_{S,i}^{\kappa\delta T_{21}}(\ell, y) = \bar{T}_b(z_i) Z_{HI}(\mathbf{k}; z_i) K_{\kappa} \left(\frac{y}{r_{\nu,i}} \right) \frac{P_{m,0} \left(\frac{\ell}{\chi_i}, \frac{y}{r_{\nu,i}} \right)}{V_p(z_i)/D(z_i)}$$

where $P_{m,0}$ is the matter power spectrum at redshift zero and $K_{\kappa}(y/r_{\nu,i})$ is the real part (due to the power spectrum symmetry) of \tilde{K}_{κ} . The key point here is that the lensing kernel is a function of y modes probed by the HI field, which do not include the lowest frequency modes ($k_{||} \lesssim k_{||,cut}$) removed in the foreground cleaning process. Indeed, in Figure 1 we see that for higher values of $k_{||,cut}$ the cross-spectrum is significantly reduced due to the rapid fall-off in K_{κ} with increasing y .

We can quantify this loss of signal in terms of the reduced signal-to-noise for the CMB and HI IM experiments considered in this paper, specifically AdvACT [44] and HIRAX [45], which will overlap over $\sim 15,000 \text{ deg}^2$, and defer the study of future surveys to a follow-up paper [46]. HIRAX is a radio interferometer array of 6m dishes currently under construction in South Africa, which will measure the HI intensity mapping signal in the 400-800 MHz band, while AdvACT was a 6m mm-wave telescope operating in Chile that made arcminute resolution maps

of the CMB. The instrument and survey specifications for these experiments given in Table I are used to specify the power spectrum noise for each experiment. For the HI IM survey the noise is given by [15]

$$C_{N,i}^{\delta T_{21}}(\ell, y) = \frac{T_{\text{sys}}^2(\tilde{\nu}_i) S_{\text{area}} \lambda^4}{\nu_{21} n_{\text{pol}} t_{\text{obs}} \text{FOV}(\tilde{\nu}_i) A_e^2 n(\mathbf{u} = \ell/2\pi)},$$

where T_{sys} is the system temperature, S_{area} is the total survey area, $\text{FOV} \approx \left(\frac{\lambda}{D_{\text{dish}}} \right)^2$ is the frequency-dependent field of view, A_e is the dish collecting area, $n_{\text{pol}} = 2$ as HIRAX will have dual polarization feeds, $t_{\text{obs}} = f_{\text{eff}} t_{\text{tot}}$ is the effective survey time, and $n(\mathbf{u})$ is the baseline density in uv coordinates. The CMB lensing noise is given by [47]

$$C_N^{\kappa}(\ell) = \frac{\ell^4}{4} \left[\int \frac{d^2 \ell'}{(2\pi)^2} \times \frac{[\ell' \cdot \ell C_S^{EB}(\ell) + (\ell - \ell') \cdot \ell C_S^{EB}(|\ell - \ell'|)^2 \sin^2(2\phi)]^{-1}}{C_{\text{tot}}^{EB}(\ell) C_{\text{tot}}^{EB}(|\ell - \ell'|)} \right]$$

where $C_{\text{tot}}^{EB}(\ell) = C_S^{EB}(\ell) + C_N^{EB}(\ell)$ and ϕ is the angle between ℓ and $\ell - \ell'$. We only consider the EB estimator since it provides a close to optimal reconstruction [48] but will consider the full lensing constraining power of more sensitive CMB surveys in a follow-up paper [46].

HIRAX HI IM	AdvACT CMB lensing
$S_{\text{area}} = 15,000 \text{ deg}^2$	$S_{\text{area}} = 15,000 \text{ deg}^2$
$t_{\text{tot}} = 4 \text{ yrs}; f_{\text{eff}} = 0.5$	Channel: 150 GHz
Bandwidth=0.4-0.8 GHz	Beam FWHM = 1.4 arcmin
$T_{\text{sys}} = 50 \text{ K}$	$T_{\text{map}} = 7 \mu\text{K-arcmin}$
$N_{\text{dish}} = 1024; D_{\text{dish}} = 6 \text{ m}$	$P_{\text{map}} = 10 \mu\text{K-arcmin}$

TABLE I: Experimental specifications for the AdvACT [44] and HIRAX [45] surveys considered in this paper.

The signal-to-noise ratio in redshift bin z_i ,

$$(\text{SNR}_i)^2 = \frac{\Delta \tilde{\nu}_i S_{\text{area}}}{2} \int_{y_{\text{min}}}^{y_{\text{max}}} \frac{dy}{(2\pi)} \int_{\ell_{\text{min}}}^{\ell_{\text{max}}} \frac{\ell d\ell}{(2\pi)} \frac{\mathcal{S}_i(\ell, y)^2}{\mathcal{V}_i(\ell, y)} \quad (1)$$

is obtained by integrating over independent transverse and radial modes with relevant volume factors. For the HI IM-CMB lensing cross-correlation the integrand, $\mathcal{S}_i(\ell, y)^2/\mathcal{V}_i(\ell, y)$, is given by

$$\frac{C_{S,i}^{\kappa\delta T_{21}}(\ell, y)^2}{C_{S,i}^{\kappa\delta T_{21}}(\ell, y)^2 + [C_S^{\kappa}(\ell) + C_N^{\kappa}(\ell)] [C_{S,i}^{\delta T_{21}}(\ell, y) + C_{N,i}^{\delta T_{21}}(\ell, y)]^2},$$

where the lensing convergence and HI IM angular power spectra are given by

$$C_{S,i}^{\delta T_{21}}(\ell, y) = \bar{T}_b^2(z_i) Z_{HI}^2(\mathbf{k}; z_i) P_m(\mathbf{k}, z_i) / V_p(z_i),$$

$$C_S^{\kappa}(\ell) = \int d\chi W_{\kappa}(\chi)^2 \frac{P_m(\mathbf{k}, \chi)}{\chi^2},$$

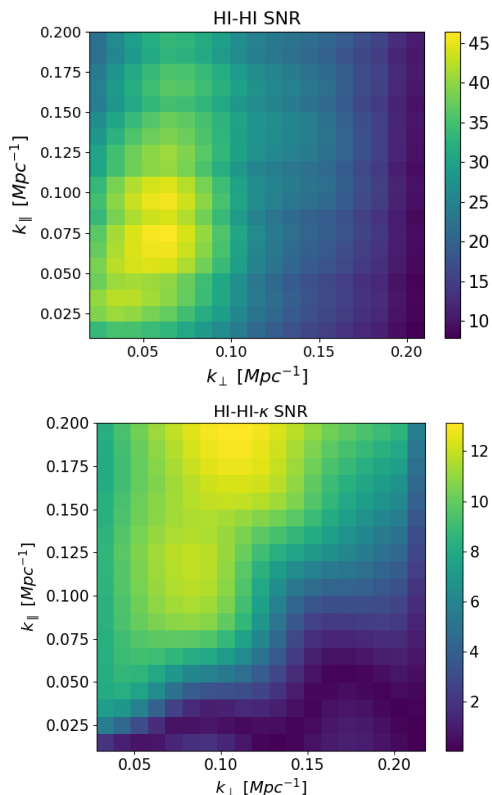


FIG. 2: Binned signal-to noise ratio (SNR) in the k_{\perp} - k_{\parallel} plane for the $z = 1.27$ redshift bin. Top panel: SNR for the HI power spectrum measured by HIRAX. Bottom panel: SNR for the cross-bispectrum measured by HIRAX and AdvACT.

and the Limber approximation is used for the CMB lensing power spectrum expression. We restrict the ℓ and y integration ranges used in this paper to the *linear* scales accessible by the HIRAX HI and AdvACT CMB lensing surveys, as described in more detail in [46]. Specifically, we find that over the HIRAX redshift range, ℓ_{min} varies from about 60 to 100, y_{min} from about 90 to 120, ℓ_{max} from about 800 to 1100, and y_{max} from about 1400 to 2000. We note that our maximum wavenumber cut-offs are chosen such that we restrict our analysis strictly to the linear regime.

In Figure 1 we show the cumulative cross-correlation SN in a given redshift bin as a function of angular modes and integrated over all radial modes, for different foreground cuts. We note that for $k_{\parallel, cut} = 0.01 \text{ Mpc}^{-1}$ the cross-correlation SNR drops by several orders of magnitude, thereby severely degrading its detectability.

A CROSS-BISPECTRUM ESTIMATOR TO RECOVER THE CROSS-CORRELATION OF HI INTENSITY MAPPING WITH CMB LENSING

We can recover the long wavelength HI modes required for the CMB lensing convergence cross-correlation by going to second order in the HI field and taking advantage of the fact that short wavelength modes are correlated in the presence of a long wavelength mode [49–51]. This *density modulation* effect results in small scale fluctuations being correlated with the large scale HI background density, which is correlated with the CMB lensing convergence. In the large-scale structure literature, this effect has been well studied in terms of super-sample modes that contribute to super-sample variance in galaxy surveys (see [52] and references therein).

In order to recover this higher order correlation with reasonable significance we require short wavelength HI modes that are well measured. This is the case for HIRAX, as seen in the top panel of Figure 2, which shows that HI power spectrum modes in the range $0.05 \lesssim k/\text{Mpc}^{-1} \lesssim 0.15$ are well measured, with $\text{SNR} \gtrsim 30$ in $(k_{\parallel}, k_{\perp})$ bins of width 0.01 Mpc^{-1} . Here the HI power spectrum SNR is given by Equation 1, with $\mathcal{S}_i^{\delta T_{21}}(\ell, y) = C_{S,i}^{\delta T_{21}}(\ell, y)$ and $\mathcal{V}_i^{\delta T_{21}}(\ell, y) = [C_{S,i}^{\delta T_{21}}(\ell, y) + C_{N,i}^{\delta T_{21}}(\ell, y)]^2$. For reference, the lensing convergence SNR is given by Equation 1, but with no y and z_i dependence, such that $\mathcal{S}_i^{\kappa}(\ell) = C_S^{\kappa}(\ell)$ and $\mathcal{V}_i^{\kappa}(\ell) = [C_S^{\kappa}(\ell) + C_N^{\kappa}(\ell)]^2$.

The cross-bispectrum estimator presented here relies on gravity-induced higher order correlations between the density field to recover the long-wavelength HI modes [49]. The bispectrum of first-order Gaussian fields vanishes, so at second order, we have $\delta T_{21}(\mathbf{k}; z_i) = \delta T_{21}^{(1)}(\mathbf{k}; z_i) + \delta T_{21}^{(2)}(\mathbf{k}; z_i)/\bar{T}_b(z_i)$, where

$$\delta T_{21}^{(2)}(\mathbf{k}, \chi) = \int \frac{d^3 q}{(2\pi)^3} Z_{HI}^{(2)}(\mathbf{q}, \mathbf{k} - \mathbf{q}, \chi) \times \frac{\delta T_{21}^{(1)}(\mathbf{k} - \mathbf{q}, \chi)}{Z_{HI}(\mathbf{k} - \mathbf{q}, \chi)} \frac{\delta T_{21}^{(1)}(\mathbf{q}, \chi)}{Z_{HI}(\mathbf{q}, \chi)}.$$

The second order redshift-space HI kernel is given by [49]

$$Z_{HI}^{(2)}(\mathbf{q}, \mathbf{k} - \mathbf{q}, \chi) = \frac{1}{2} b_{HI}^{(2)}(\chi) + \frac{1}{2} f(\chi) k_{\parallel} \times \left[\frac{\mu_1}{q_1} \left(b_{HI}^{(1)}(\chi) + f(\chi) \mu_2^2 \right) + \frac{\mu_2}{q_2} \left(b_{HI}^{(1)}(\chi) + f(\chi) \mu_1^2 \right) \right] + b_{HI}^{(1)}(\chi) F_2(\mathbf{q}, \mathbf{k} - \mathbf{q}) + f(\chi) \left(\frac{k_{\parallel}}{k} \right)^2 G_2(\mathbf{q}, \mathbf{k} - \mathbf{q})$$

with

$$\begin{aligned} \mu_1 &= \frac{q_{\parallel}}{q_1}, \quad q_1 = |\mathbf{q}|; \quad \mu_2 = \frac{k_{\parallel} - q_{\parallel}}{q_2}, \quad q_2 = |\mathbf{k} - \mathbf{q}|, \\ F_2(\mathbf{k}_1, \mathbf{k}_2) &= \frac{5}{7} + \frac{2}{7} \frac{(\mathbf{k}_1 \cdot \mathbf{k}_2)^2}{k_1^2 k_2^2} + \frac{1}{2} \frac{\mathbf{k}_1 \cdot \mathbf{k}_2}{k_1 k_2} \left(\frac{k_1}{k_2} + \frac{k_2}{k_1} \right), \\ G_2(\mathbf{k}_1, \mathbf{k}_2) &= \frac{3}{7} + \frac{4}{7} \frac{(\mathbf{k}_1 \cdot \mathbf{k}_2)^2}{k_1^2 k_2^2} + \frac{1}{2} \frac{\mathbf{k}_1 \cdot \mathbf{k}_2}{k_1 k_2} \left(\frac{k_1}{k_2} + \frac{k_2}{k_1} \right), \end{aligned}$$

where the F_2 kernel given in [49] has been corrected (see e.g., [53]). For the HI bias we use the redshift dependent form for $b_{HI}^{(1)}$ and $b_{HI}^{(2)}$ from [54]. In the above we ignore higher order non-linear corrections to $Z_{HI}^{(2)}$ [49, 55] as these effects are sub-dominant for the linear scales we consider here and in the squeezed limit these terms, including the tidal bias, vanish exactly [46]. As indicated above, in this study we restrict ourselves to linear HI and CMB lensing modes that contribute to the bispectrum.

We choose to correlate the power spectrum of the local HI temperature field, the so-called position-dependent HI power spectrum,

$$P_{21}(\mathbf{k}; z_i)|_{\mathbf{r}} = \frac{1}{V_L} \delta T_{21}(\mathbf{k}; z_i)|_{\mathbf{r}} \delta T_{21}^*(\mathbf{k}; z_i)|_{\mathbf{r}}$$

in some volume, $V_L(z_i) = L_{\parallel} L_{\perp}^2 = \Omega_i \Delta \tilde{v}_i V_p(z_i)$, centred at position \mathbf{r} in redshift bin z_i , with the mean density of that volume, as traced by the CMB lensing convergence field, κ . As discussed in [50], this correlation defines an integrated bispectrum. The position-dependent power spectrum probes coupling between large-scale and small-scale modes by measuring the local power spectrum, which is correlated with the mean density in that volume.

Here the local HI field in the volume (up to second order) is given by

$$\delta T_{21}(\mathbf{k}; z_i)|_{\mathbf{r}} = V_L \int \frac{d^3 k_1}{(2\pi)^3} e^{-i\mathbf{k}_1 \cdot \mathbf{r}} W_L^{21}(\mathbf{k}_1) \delta T_{21}(\mathbf{k} - \mathbf{k}_1; z_i)$$

where we choose top-hat window functions in position space, corresponding to sinc functions in harmonic space, $W_L(q) = \text{sinc}(q)$. The average CMB lensing convergence in the volume is obtained by transforming the lensing convergence, $\kappa(\boldsymbol{\theta}; z_i)$, and taking the $\ell = 0$ mode, which gives

$$\bar{\kappa}(z_i)|_{\mathbf{r}} = \frac{V_L W_{\kappa}(\chi_i)}{\chi_i^2} \int \frac{d^3 q'}{(2\pi)^3} e^{-i\mathbf{r} \cdot \mathbf{q}'} W_L^{\kappa}(\mathbf{q}') \delta_m(-\mathbf{q}'; z_i).$$

The correlation of the HI position-dependent power spectrum with the average CMB convergence within the volume defines the HI-HI- κ cross-bispectrum

$$B_{S,i}^{\bar{\kappa} \delta T_{21} \delta T_{21}}(\ell, y; z_i) = \langle P_{21}(\mathbf{k}; z_i)|_{\mathbf{r}} \bar{\kappa}(z_i)|_{\mathbf{r}} \rangle.$$

where the expectation value is taken over all sub-volumes across the survey region in a given redshift bin. The HI-HI- κ cross-bispectrum is dominated by squeezed configurations [50] for the large HI wavenumbers of interest to

us. In [46] we derive the expression for the full cross-bispectrum, but here we focus on its squeezed limit analogue. We find that in the squeezed limit the HI-HI- κ cross-bispectrum in redshift bin, z_i , reduces to [46]

$$\begin{aligned} B_{S,i}^{\bar{\kappa} \delta T_{21} \delta T_{21}}(\ell, y) &= \frac{\Omega_i \Delta \tilde{v}_i W_{\kappa}(\chi_i)}{\chi_i^2} P_{21}(\mathbf{k}, z_i) \left\{ \frac{1 + f(\chi_i) \mu_k^2}{2} \times \right. \\ &\left. \left(3 - \frac{d \log P_m}{d \log k} \right) + \frac{b_{HI}^{(2)}(\chi_i) + (4\mu_k^2 - 2)(f(\chi_i) + f^2(\chi_i) \mu_k^2)}{b_{HI}^{(1)}(\chi_i) + f(\chi_i) \mu_k^2} \right\} \\ &\times \int \frac{d^3 q}{(2\pi)^3} W_L^{\kappa}(\mathbf{q}) W_L^{21}(\mathbf{q}) P_m(\mathbf{q}; z_i). \end{aligned}$$

As noted in the literature [50, 56], the squeezed-limit bispectrum probes the linear response of the small-scale power spectrum, P_{21} , to the variance of the large-scale fluctuations, captured by the integral over P_m , with the response function for the HI-HI- κ cross-bispectrum given in curly brackets above, and the overall normalisation set by appropriate projection and volume factors.

The HI-HI- κ cross-bispectrum signal-to-noise ratio is given by Equation 1, where $\mathcal{S}_i(\ell, y) = B_{S,i}^{\bar{\kappa} \delta T_{21} \delta T_{21}}(\ell, y; z_i)$ and $\mathcal{V}_i(\ell, y) = 2\mathcal{V}_i^{\delta T_{21}}(\ell, y) \mathcal{V}_i^{\kappa}(\ell)$ is the variance. We have found that the Gaussian contribution dominates the diagonal covariance, over the diagonal covariance term containing the HI- κ two-point correlation, which we have shown is negligible, and over the diagonal contributions from the non-Gaussian ‘BB’ and ‘PT’ covariance terms, which can be significant for squeezed bispectra [57–59]. These terms are smaller than the Gaussian covariance term on large angular scales due to the Gaussian signal term dominating, as can be seen in [57], and on small angular scales due to the dominant lensing reconstruction and HI noise [46]. Off-diagonal contributions from the ‘BB’ and ‘PT’ terms are also small relative to the diagonal Gaussian contribution, but could affect cosmological parameter correlations in a nontrivial way. We have perturbatively included the off-diagonal contribution from the ‘BB’ term (which dominates over the ‘PT’ term on the scales we are interested in) and found negligible changes to the parameter constraints presented in the next section. A more detailed study of the cross-bispectrum covariance is presented in [46].

From the bottom panel of Figure 2 we see that the HI-HI- κ cross-bispectrum is detectable with high significance, assuming HIRAX and AdvACT specifications, for a large range of radial and transverse modes. This is true even in the presence of the HI foreground cut, unlike the cross-power spectrum. Furthermore, it is evident from the bottom panel of Figure 2 that the cross-bispectrum estimator is fairly robust to the removal of foreground modes since the SNR is mainly contributed by scales outside the foreground wedge [60]. Even when a conservative horizon-scale foreground wedge cut is applied we find that the total SNR in the $z = 1.27$ bin only drops by about 10% (from 156 to 139).

PARAMETER FORECASTS

We forecast parameter constraints using the Fisher matrix given by

$$F_{ab,i} = \frac{1}{2} S_{\text{area}} \Delta \tilde{\nu}_i \int \frac{d^2 \ell}{(2\pi)^2} \int \frac{dy}{(2\pi)} \frac{\partial_{p_a} \mathcal{S}_i(\ell, y) \partial_{p_b} \mathcal{S}_i(\ell, y)}{\mathcal{V}_i(\ell, y)}$$

in redshift bin, z_i [15, 61]. The signal spectra are $\mathcal{S}_i = \{C_{S,i}^{\delta T_{21}}(\ell, y), C_{S,i}^{\kappa}(\ell), B_{S,i}^{\bar{\kappa} \delta T_{21} \delta T_{21}}(\ell, y)\}$ and we use the diagonal covariance $\mathcal{V}_i(\ell, y)$ for each of the probes given in the previous section. We combine constraints from the different power spectra and bispectra signals, and in different redshift bins, by adding the relevant Fisher matrices, because the cross-probe covariances are negligible, as argued above.

Given the Fisher matrix, F_{ab} , the marginalised error on parameter a is given by $\delta p_a = \sqrt{(F^{-1})_{aa}}$. We include *Planck* priors from the temperature and polarization power spectra (not including lensing) with all our combined probes. The covariance between CMB lensing and the temperature and polarization constraints is negligible [62]. We pre-marginalize over τ in the *Planck* priors.

Redshift-dependent quantities

We first vary the redshift-dependent quantities, $A_{\text{bao}}, \sigma_8, f\Omega_{\text{HI}}, b_{\text{HI}}^{(1)}\Omega_{\text{HI}}, b_{\text{HI}}^{(2)}\Omega_{\text{HI}}, d_A$, and H , but focus on constraints on f and σ_8 below, marginalizing over the other quantities in each redshift bin. We allow these functions to vary in each redshift bin with their fiducial value fixed by its functional form. The amplitude of the baryon acoustic oscillations, A_{bao} , we obtain by defining $f_{\text{bao}}(k)$ such that $P(k) = [1 + A_{\text{bao}} f_{\text{bao}}(k)] P_{\text{smooth}}(k)$ [15]. We vary the amplitude of the matter power spectrum, σ_8 , such that $P_m(k) = (\sigma_8/\sigma_8^{\text{fid}})^2 P_m^{\text{fid}}(k)$. The linear growth function is given by $f(z) = \Omega_m(z)^\gamma$, where the growth index parameter is $\gamma = 0.55$ for the Λ CDM model within general relativity [63], which we use as our fiducial model. The combination of the HI intensity mapping and lensing convergence is unable to constrain Ω_{HI} independently, hence the factor, Ω_{HI} , is included in combination with some of our parameters. The constraints in this section include a $k_{\parallel, \text{cut}}$ foreground cut.

The top panel of Figure 3 shows the constraints on $f\Omega_{\text{HI}}$ and σ_8 in a single redshift bin (centred at $z = 1.27$) from the HI and lensing convergence power spectra and the cross-bispectrum, where we have marginalized over the bias parameters. The cross-bispectrum helps to break the degeneracy between $f\Omega_{\text{HI}}$ and σ_8 in the HI power spectrum, because the bispectrum signal contains added information on σ_8 from the CMB lensing contribution. This contribution to the bispectrum signal adds a fourth power dependence on σ_8 in the bispectrum expression

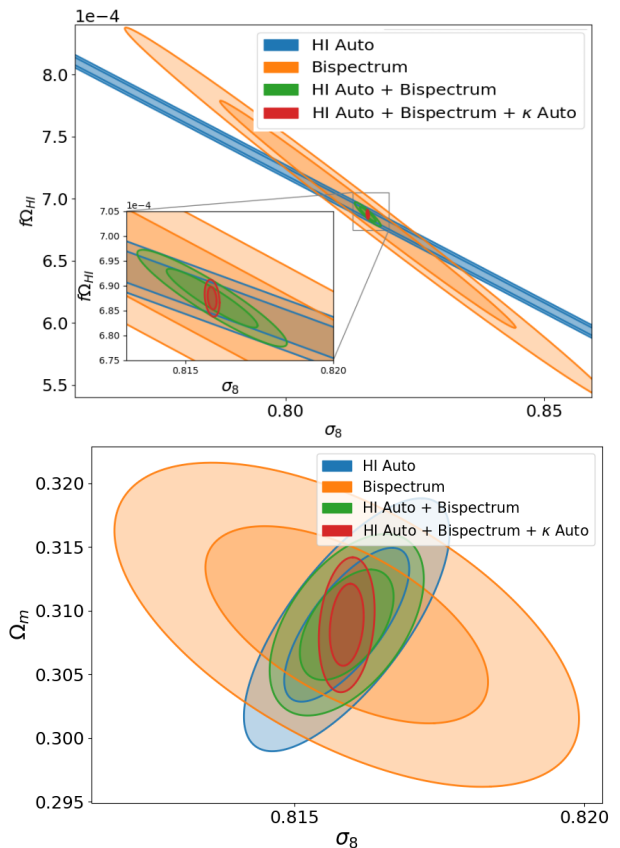


FIG. 3: Forecast 1σ and 2σ constraints on f and σ_8 (top panel), and Ω_m and σ_8 (bottom panel), from HIRAX HI and AdvACT lensing, in the redshift bin centred at $z = 1.27$, for different power spectrum and cross-bispectrum combinations. This is one of four redshift bins spanning the HIRAX redshift range. The bispectrum has a different degeneracy direction to the HI power spectrum in the f - σ_8 plane. The lensing power spectrum further constrains σ_8 .

versus the squared dependence on σ_8 present in HI auto-correlation expression. The lensing power spectrum also provides a constraint on σ_8 that further helps to break this degeneracy.

Measurements of f and σ_8 have been reported in [64, 65]. In these respective references, they combine galaxy counts and galaxy-galaxy lensing to break the f and σ_8 degeneracy. The state-of-the-art constraints from these measurements place an error of 0.22 on f and 0.06 on σ_8 . In contrast, our forecasts are 36 times better on $f\Omega_{\text{HI}}$ and 300 times better on σ_8 in the redshift bin centred at $z = 1.27$. Our forecasts improve on these measurements and the forecast constraints given in Ref. [66] where the BOSS galaxy bispectrum and power spectrum have been used in combination to break the f - σ_8 parameter degeneracy placing $\sim 4\%$ errors on these parameters. More recent forecasts have been presented in Refs. [67] and [68], where they combine the galaxy power spectrum with phased redshift-space correlations or the

galaxy bispectrum, respectively, to break the f - σ_8 degeneracy, obtaining 3% and 1% errors on f and 0.5% and 1% errors on σ_8 respectively. We can achieve constraints of 1.6% on $f\Omega_{HI}$ and 0.2% on σ_8 in the above redshift bin by combining the bispectrum information with the HI power spectrum. Adding lensing and considering all four redshift bins, $z = (0.81, 0.95, 1.27, 1.95)$, reduces these to sub-percent constraints of (0.8%, 0.75%, 0.6%, 0.7%) on $f\Omega_{HI}$ and (0.023%, 0.031%, 0.02%, 0.038%) on σ_8 , respectively.

Λ CDM parameters

The parameter set we consider for the vanilla Λ CDM case is $\{\Omega_m, \sigma_8, h, n_s, \Omega_b\}$, where we marginalize over the HI biases and A_{bao} in each redshift bin, retaining constraints on f, d_A, H and σ_8 . We use the width of the *Planck* 2018 priors from the corresponding model [40].

For cosmological constraints, we introduce the distance scale parameters, $\alpha_\perp = D_A^{\text{fid}}(z)/D_A(z)$ and $\alpha_\parallel = H(z)/H^{\text{fid}}(z)$, [69], where the angular diameter distance, D_A , and the expansion rate, H , respectively, measure the distance in the transverse and radial directions. We then introduce distance scale parameters into our model by re-scaling the harmonic wavenumbers such that $\ell \rightarrow \alpha_\perp \ell$ and $y \rightarrow \alpha_\parallel y$. We can then transform the Fisher matrix with the implicit redshift dependent functions and distance scale parameters, F_{ij} , to the Fisher matrix containing the cosmological parameters, F'_{ij} , by

$$[F'_{ij}] = [M_{ij}]^T [F_{ij}] [M_{ij}] \quad (2)$$

where $M_{ij} = \partial_{p_i}/\partial_{p'_j}$ is the transformation matrix. The constraints on $\Omega_{m,0}$ and $\sigma_{8,0}$, dropping the subscript ‘0’ hereafter, after marginalizing over the other parameters are shown in the bottom panel of Figure 3. The Ω_m - σ_8 figure of merit [70] for this constraint is $\text{FOM}_{\Omega_m\sigma_8} = 80000$. This can be compared to the DES Y3 constraints, which have $\text{FOM}_{\Omega_m\sigma_8} \sim 2000 - 3000$ for DES data alone and $\text{FOM}_{\Omega_m\sigma_8} \sim 34041$ for the DES Y3 3x2pt analysis combined with external data [70]. We would therefore improve by a factor of two over current constraints.

The errors on the Λ CDM parameters are shown in Table II. The constraint on Ω_m can be converted to a constraint on Ω_Λ . The biggest improvements from HI data alone are for σ_8 and n_s , although constraints on Ω_m and h also improve. Adding the bispectrum and lensing power spectrum makes the most significant difference to σ_8 and n_s . These constraints include a $k_{\parallel, \text{cut}}$ foreground cut.

Dark Energy Equation of State

In addition to the Λ CDM parameters we now include a parameterization of a varying dark energy equation of state [71, 72], $w = w_0 + w_a(1 - a)$, where

	Ω_m	σ_8	h	n_s	ω_b
<i>Planck</i>	0.0074	0.0060	0.0054	0.0042	0.00015
HIRAX HI + <i>Planck</i>	0.0041	0.00073	0.0031	0.0012	0.00012
Combined + <i>Planck</i>	0.0022	0.00020	0.0017	0.00059	0.00011

TABLE II: Marginalized 68% cosmological parameter forecasts for the HI power spectrum and the combined constraint, that includes, in addition, the CMB lensing power spectrum and HI-CMB lensing cross-bispectrum, all with *Planck* priors.

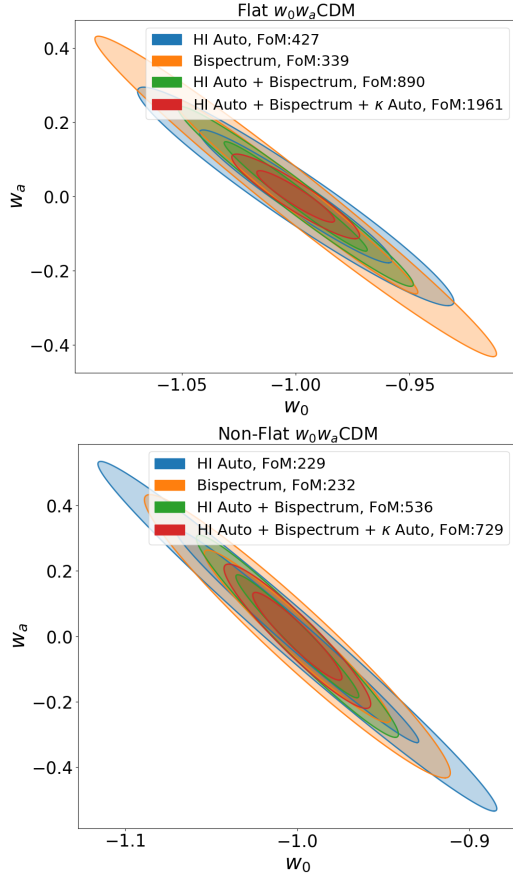


FIG. 4: Forecast 1σ and 2σ constraints on w_0 and w_a from HIRAX HI and AdvACT lensing for different power spectrum and cross-bispectrum combinations. Top panel: Flat w_0w_a CDM model with fixed $\Omega_K = 0$. Bottom panel: Non-flat w_0w_a CDM model, marginalizing over Ω_K .

a is the scale factor. We vary the parameter set $\{w_0, w_a, \Omega_m, \sigma_8, h, n_s, \omega_b\}$, where we marginalize over the HI biases in each redshift bin. We again incorporate *Planck* 2018 priors.

In Table III we quote the marginalised errors on a subset of cosmological parameters, assuming *Planck* priors. We again see significant improvement in the parameter forecasts by combining all probes compared to the HI case. These constraints include a $k_{\parallel, \text{cut}}$ foreground cut and a wedge cut, showing that our estimator is indeed robust to foregrounds, because small-scale HI modes

contribute most to the cross-bispectrum SNR. We have confirmed that the results without a $k_{\parallel, cut}$ foreground cut are only marginally ($\sim 0.1\%$) better. The combined cross-bispectrum probes are able to constrain dark energy equation of state parameters w_0 and w_a at the 1.4% and 6% level, respectively, without curvature, and at the 2.2% and 9% level, respectively, when varying curvature. The current state-of-the-art constraints obtained from the eBOSS cosmology analysis, combined with constraints from Planck, Pantheon SNe Ia and DES Y1 on dark energy equation of state parameters are 7% and 50% constraints on w_0 and w_a , respectively [73].

Figure 4 shows the marginalized forecasts for the dark energy equation of state parameters, where we have quoted constraints on Ω_Λ in place of Ω_m . The top panel shows the dark energy constraints if the curvature Ω_K is fixed to its fiducial value rather than marginalized over. The constraints on dark energy are not severely degraded when Ω_K is varied. As seen in the bottom panel of Figure 4, the dark energy FoM of ~ 500 (HI power spectrum and bispectrum) and ~ 700 (all probes combined) improves significantly on current constraints, even without prior knowledge of curvature.

Combining the auto-correlation probes with the cross-bispectrum produces tighter parameter constraints as there is a slight offset in the $w_0 - w_a$ degeneracy directions between the probes, caused by the differing contributions of growth and distance scale parameters to each probe. The cross-bispectrum helps break CMB lensing degeneracies, improving CMB lensing constraints by a factor of two on w_0 , w_a , and Ω_Λ in the flat model and on Ω_K in the curved model.

Our combined dark energy constraints are competitive with other large-scale structure forecasts such as SKA [74], and DESI [75], where we note that our combined figure of merit is larger by at least a factor of 3. Forecasts on joint SKA1-Mid surveys with Planck priors [74] yield a 7% and 34% constraint on these parameters, respectively. Forecasts for DESI [76] place a 1% error on w_p , the pivot value for $w(a)$. Forecasts for Euclid [77] including Planck and future CMB lensing priors, which are the most competitive with our constraints, quote 2.1% and 7.3% flat-model constraints on w_0 and w_a , respectively, with curved model constraints at the 2.1% and 8.6% level.

DISCUSSION

In this paper we have developed a new cross-bispectrum estimator that recovers correlations between HI intensity mapping surveys and projected cosmological fields like CMB secondary anisotropies, which are negligible for the cross-power spectrum due to removal of foreground modes in the 21cm maps. We have applied this estimator to the cross-correlation between HI

	Ω_K	Ω_Λ	w_0	w_a	h
HIRAX HI + <i>Planck</i>	–	0.0022	0.025	0.09	0.0022
AdvACT lensing + <i>Planck</i>	–	0.0041	0.028	0.11	0.0027
Combined + <i>Planck</i>	–	0.0020	0.014	0.06	0.0021
HIRAX HI + <i>Planck</i>	0.0037	0.0058	0.031	0.13	0.0044
AdvACT lensing + <i>Planck</i>	0.0063	0.0062	0.039	0.11	0.0056
Combined + <i>Planck</i>	0.0031	0.0056	0.022	0.09	0.0042

TABLE III: Marginalized 68% cosmological parameter forecasts for the HI power spectrum, the CMB lensing power spectrum and the combined constraint, that includes, in addition to these two power spectra, the HI-CMB lensing cross-bispectrum. All forecasts include Planck priors.

intensity mapping and CMB lensing, and studied the cross-bispectrum detectability and resulting cosmological parameter constraints, specifically for HIRAX and AdvACT. We found that the cross-bispectrum is detected with high significance and provides complementary information to the HI IM auto and CMB lensing power spectra that breaks degeneracies between key cosmological parameters. When combined with these probes, it provides cosmological parameter constraints that are very competitive with future surveys, in particular on the dark energy equation of state, the growth function and amplitude of small-scale fluctuations. Moreover, we established that the HI-CMB lensing cross-bispectrum is robust to foreground removal, including the removal of wedge modes, as it relies primarily on well-measured small-scale line-of-sight HI modes, which HIRAX will provide.

In addition to constraints on the standard cosmological parameters, the bispectrum also provides competitive constraints on extended model parameters beyond the $w_0 w_a$ CDM model considered above, which we explore in more detail in [46]. Here, we extend the $w_0 w_a \Omega_K$ CDM model to include the sum of neutrino masses as a parameter that we vary in the Fisher matrix, and find a $1-\sigma$ constraint on the neutrino mass sum of 5.5 meV. This is very competitive with combined bispectrum and power spectrum constraints from future large-scale structure and CMB surveys, or multi-tracer power spectrum constraints from these surveys. In [78] they forecast a 16 meV neutrino mass constraint using CMB-S4 combined with a DESI BAO survey, while power spectrum forecasts from a multi-tracer HI IM and CMB survey constrains the neutrino mass at 11 meV [79], in models with a more restricted parameter set. This indicates that the cross-bispectrum is a powerful probe of cosmology in combination with its corresponding auto spectra, and will be even more so [46] if one uses future HI IM surveys e.g. PUMA [80] and CMB lensing surveys e.g. from Simons Observatory (SO) and CMB-S4 (S4) [81, 82].

There are a few assumptions we have made in this paper that could be explored further. We have restricted our analysis to linear scales but there is additional infor-

mation in nonlinear modes beyond these scales, however, the modelling and interpretation become more complicated. Apart from the second-order bias correction, we have ignored non-linear corrections to the HI signal, including the non-local tidal term, but we include these terms in a follow-up paper [46], where we show that, under the squeezed approximation, these higher-order terms vanish. Including nonlinear modes also necessitates a more detailed modelling of the signal covariance terms. For simplicity, we have only considered the squeezed limit of the cross-bispectrum. In principle, more information exists in other bispectrum configurations but in [51] the authors have shown that the squeezed limit dominates the information content of the cross-bispectrum. We have used a specific model for the HI bias from [54] but could explore the impact of other models for the HI bias.

There are various future avenues of research related to the HI cross-bispectrum correlation with CMB or LSS probes. In a follow-up paper [46], we study the bispectrum signal and covariance in detail, and consider how well future HI IM surveys, such as SKA and PUMA, and future CMB lensing surveys such as SO and S4, will measure the HI-CMB lensing cross-bispectrum and constrain parameters, including constraints on non-standard cosmological parameters such as primordial non-gaussianity, the sum of neutrino masses, and modified gravity models. In a separate paper [83], we study the HI-CMB lensing cross-bispectrum signal in the epoch of reionisation. We also leave for future work studies of HI bispectrum cross-correlations with other large-scale structure probes, such as photometric galaxy and cosmic shear surveys [84], and CMB secondary signals such as the Sunyaev-Zel'dovich effect [85] and the cosmic infrared background [86].

Acknowledgements: We acknowledge useful discussions with Devin Crichton, Martin Bucher, Pedro Ferreira, David Alonso, Roy Maartens, Louis Perenon, Francisco Villaescusa-Navarro, David Spergel, Will Coulton, and Oliver Philcox. We acknowledge visitor and sabbatical support from the Simons Foundation, where part of this work was completed. KM acknowledges support from the National Research Foundation of South Africa and the Fulbright Scholar Program. WN acknowledges support from the South African Radio Astronomy Observatory.

* Electronic address: moodleyk41@ukzn.ac.za

- [1] D. N. Spergel, L. Verde, H. V. Peiris, E. Komatsu, M. Nolta, C. L. Bennett, M. Halpern, G. Hinshaw, N. Jarosik, A. Kogut, et al., *The Astrophysical Journal Supplement Series* **148**, 175 (2003).
- [2] P. A. Ade, N. Aghanim, M. Arnaud, M. Ashdown, J. Aumont, C. Baccigalupi, A. Banday, R. Barreiro, J. Bartlett, N. Bartolo, et al., *Astronomy & Astrophysics* **594**, A13 (2016).
- [3] S. Das, B. D. Sherwin, P. Aguirre, J. W. Appel, J. R. Bond, C. S. Carvalho, M. J. Devlin, J. Dunkley, R. Dünner, T. Essinger-Hileman, et al., *Physical Review Letters* **107**, 021301 (2011).
- [4] J. Ruhl, P. A. Ade, J. E. Carlstrom, H.-M. Cho, T. Crawford, M. Dobbs, C. H. Greer, W. L. Holzapfel, T. M. Lanting, A. T. Lee, et al., in *Millimeter and Submillimeter Detectors for Astronomy II* (SPIE, 2004), vol. 5498, pp. 11–29.
- [5] M. Levi, C. Bebek, T. Beers, R. Blum, R. Cahn, D. Eisenstein, B. Flaugher, K. Honscheid, R. Kron, O. Lahav, et al., arXiv preprint arXiv:1308.0847 (2013).
- [6] D. Spergel, N. Gehrels, C. Baltay, D. Bennett, J. Breckinridge, M. Donahue, A. Dressler, B. Gaudi, T. Greene, O. Guyon, et al., arXiv preprint arXiv:1503.03757 (2015).
- [7] R. Laureijs, J. Amiaux, S. Arduini, J.-L. Augueres, J. Brinchmann, R. Cole, M. Cropper, C. Dabin, L. Duvet, A. Ealet, et al., arXiv preprint arXiv:1110.3193 (2011).
- [8] R. Battye, M. Brown, I. Browne, R. Davis, P. Dewdney, C. Dickinson, G. Heron, B. Maffei, A. Pourtsidou, and P. Wilkinson, arXiv preprint arXiv:1209.1041 (2012).
- [9] K. Bandura, G. E. Addison, M. Amiri, J. R. Bond, D. Campbell-Wilson, L. Connor, J.-F. Cliche, G. Davis, M. Deng, N. Denman, et al., in *Ground-based and Airborne Telescopes V* (International Society for Optics and Photonics, 2014), vol. 9145, p. 914522.
- [10] J. L. Jonas, *Proceedings of the IEEE* **97**, 1522 (2009).
- [11] C. Carilli and S. Rawlings, arXiv preprint astro-ph/0409274 (2004).
- [12] X. Chen, in *International Journal of Modern Physics: Conference Series* (World Scientific, 2012), vol. 12, pp. 256–263.
- [13] D. Crichton, M. Aich, A. Amara, K. Bandura, B. A. Bassett, C. Bengaly, P. Berner, S. Bhatporia, M. Bucher, T.-C. Chang, et al., *Journal of Astronomical Telescopes, Instruments, and Systems* **8**, 011019 (2022).
- [14] K. Vanderlinde, K. Bandura, L. Belostotski, R. Bond, P. Boyle, J. Brown, H. Chiang, M. Dobbs, B. Gaensler, G. Hinshaw, et al., arXiv preprint arXiv:1911.01777 (2019).
- [15] P. Bull, P. G. Ferreira, P. Patel, and M. G. Santos, *The Astrophysical Journal* **803**, 21 (2015).
- [16] J. R. Shaw, K. Sigurdson, U.-L. Pen, A. Stebbins, and M. Sitwell, *The Astrophysical Journal* **781**, 57 (2014).
- [17] M. G. Santos, P. Bull, D. Alonso, S. Camera, P. G. Ferreira, G. Bernardi, R. Maartens, M. Viel, F. Villaescusa-Navarro, F. B. Abdalla, et al., arXiv preprint arXiv:1501.03989 (2015).
- [18] S. Camera, M. G. Santos, P. G. Ferreira, and L. Ferramacho, *Physical Review Letters* **111**, 171302 (2013).
- [19] A. Liu and J. R. Shaw, *Publications of the Astronomical Society of the Pacific* **132**, 062001 (2020).
- [20] M. G. Santos, A. Cooray, and L. Knox, *The Astrophysical Journal* **625**, 575 (2005).
- [21] A. Liu, J. R. Pritchard, M. Tegmark, and A. Loeb, *Physical Review D* **87**, 043002 (2013).
- [22] J. R. Shaw, K. Sigurdson, M. Sitwell, A. Stebbins, and U.-L. Pen, *Physical Review D* **91**, 083514 (2015).
- [23] E. R. Switzer and A. Liu, *The Astrophysical Journal* **793**, 102 (2014).
- [24] S. Paul, M. G. Santos, Z. Chen, and L. Wolz, arXiv preprint arXiv:2301.11943 (2023).
- [25] T.-C. Chang, U.-L. Pen, K. Bandura, and J. B. Peterson, arXiv preprint arXiv:1007.3709 (2010).
- [26] K. Masui, E. Switzer, N. Banavar, K. Bandura, C. Blake,

- L.-M. Calin, T.-C. Chang, X. Chen, Y.-C. Li, Y.-W. Liao, et al., *The Astrophysical Journal Letters* **763**, L20 (2013).
- [27] M. Raffei-Ravandi, K. M. Smith, D. Li, K. W. Masui, A. Josephy, M. Dobbs, D. Lang, M. Bhardwaj, C. Patel, K. Bandura, et al., *The Astrophysical Journal* **922**, 42 (2021).
- [28] L. Wolz, C. Tonini, C. Blake, and J. Wyithe, *Monthly Notices of the Royal Astronomical Society* **458**, 3399 (2016).
- [29] A. Pourtsidou, D. Bacon, R. Crittenden, and R. B. Metcalf, *Monthly Notices of the Royal Astronomical Society* **459**, 863 (2016).
- [30] A. Pourtsidou, D. Bacon, and R. Crittenden, *Physical Review D* **92**, 103506 (2015).
- [31] R. Ansari, E. J. Arena, K. Bandura, P. Bull, E. Castorina, T.-C. Chang, S. Foreman, J. Frisch, D. Green, D. Karagiannis, et al., arXiv preprint arXiv:1810.09572 (2018).
- [32] F. Shi, Y.-S. Song, J. Asorey, D. Parkinson, K. Ahn, J. Yao, L. Zhang, and S. Zuo, *Monthly Notices of the Royal Astronomical Society* **499**, 4613 (2020).
- [33] T. G. Sarkar, K. K. Datta, and S. Bharadwaj, *Journal of Cosmology and Astroparticle Physics* **2009**, 019–019 (2009), ISSN 1475-7516, URL <http://dx.doi.org/10.1088/1475-7516/2009/08/019>.
- [34] S. Tanaka, S. Yoshiura, K. Kubota, K. Takahashi, A. J. Nishizawa, and N. Sugiyama, arXiv preprint arXiv:1904.10363 (2019).
- [35] T. G. Sarkar, K. Datta, A. Pal, T. R. Choudhury, and S. Bharadwaj, *Journal of Astrophysics and Astronomy* **37**, 26 (2016).
- [36] A. Pourtsidou, D. Bacon, and R. Crittenden, *Monthly Notices of the Royal Astronomical Society* **470**, 4251 (2017).
- [37] H.-M. Zhu, U.-L. Pen, Y. Yu, X. Er, and X. Chen, *Physical Review D* **93**, 103504 (2016).
- [38] N. G. Karaçaylı and N. Padmanabhan, *Monthly Notices of the Royal Astronomical Society* **486**, 3864 (2019).
- [39] H.-M. Zhu, T.-X. Mao, and U.-L. Pen, *The Astrophysical Journal* **929**, 5 (2022).
- [40] N. Aghanim, Y. Akrami, M. Ashdown, J. Aumont, C. Baccigalupi, M. Ballardini, A. Banday, R. Barreiro, N. Bartolo, S. Basak, et al., *Astronomy & Astrophysics* **641**, A6 (2020).
- [41] K. M. Smith, M. S. Madhavacheril, M. Münchmeyer, S. Ferraro, U. Giri, and M. C. Johnson, arXiv preprint arXiv:1810.13423 (2018).
- [42] X. Wang, M. Tegmark, M. G. Santos, and L. Knox, *The Astrophysical Journal* **650**, 529 (2006).
- [43] A. Lewis and A. Challinor, *Physics Reports* **429**, 1 (2006).
- [44] S. W. Henderson, R. Allison, J. Austermann, T. Baildon, N. Battaglia, J. A. Beall, D. Becker, F. De Bernardis, J. R. Bond, E. Calabrese, et al., *Journal of Low Temperature Physics* **184**, 772–779 (2016), ISSN 1573-7357, URL <http://dx.doi.org/10.1007/s10909-016-1575-z>.
- [45] L. Newburgh, K. Bandura, M. Bucher, T.-C. Chang, H. Chiang, J. Cliche, R. Davé, M. Dobbs, C. Clarkson, K. Ganga, et al., in *Ground-based and Airborne Telescopes VI* (International Society for Optics and Photonics, 2016), vol. 9906, p. 99065X.
- [46] N. Warren, M. Kavilan, P. Heather, P. Louis, and M. Roy, *Journal of Cosmology and Astroparticle Physics*, *In prep.* (2022).
- [47] W. Hu and T. Okamoto, *The Astrophysical Journal* **574**, 566 (2002).
- [48] T. Okamoto and W. Hu, *Physical Review D* **67**, 083002 (2003).
- [49] F. Bernardeau, S. Colombi, E. Gaztanaga, and R. Scoccimarro, *Physics reports* **367**, 1 (2002).
- [50] C.-T. Chiang, C. Wagner, F. Schmidt, and E. Komatsu, *Journal of Cosmology and Astroparticle Physics* **2014**, 048 (2014).
- [51] C.-T. Chiang, arXiv preprint arXiv:1508.03256 (2015).
- [52] M. Takada and W. Hu, *Physical Review D* **87**, 123504 (2013).
- [53] D. Munshi and P. Coles, *Journal of Cosmology and Astroparticle Physics* **2017**, 010 (2017).
- [54] A. Pénin, O. Umeh, and M. G. Santos, *Monthly Notices of the Royal Astronomical Society* **473**, 4297 (2018).
- [55] D. Karagiannis, A. Slosar, and M. Liguori, *Journal of Cosmology and Astroparticle Physics* **2020**, 052 (2020).
- [56] C. Doux, E. Schaan, E. Aubourg, K. Ganga, K.-G. Lee, D. N. Spergel, and J. Tréguer, *Physical Review D* **94**, 103506 (2016).
- [57] A. Barreira, *Journal of Cosmology and Astroparticle Physics* **2019**, 008 (2019).
- [58] M. Biagetti, L. Castiblanco, J. Noreña, and E. Sefusatti, arXiv preprint arXiv:2111.05887 (2021).
- [59] T. Flöss, M. Biagetti, and P. D. Meerburg, arXiv preprint arXiv:2206.10458 (2022).
- [60] D. Alonso, P. G. Ferreira, M. J. Jarvis, and K. Moodley, *Physical Review D* **96**, 043515 (2017).
- [61] M. Tegmark, *Physical Review Letters* **79**, 3806 (1997).
- [62] M. M. Schmittfull, A. Challinor, D. Hanson, and A. Lewis, *Physical Review D* **88**, 063012 (2013).
- [63] E. V. Linder, *Phys. Rev. D* **72**, 043529 (2005), astro-ph/0507263.
- [64] S. De La Torre, E. Jullo, C. Giocoli, A. Pezzotta, J. Bel, B. Granett, L. Guzzo, B. Garilli, M. Scodeggio, M. Bolzonella, et al., *Astronomy & Astrophysics* **608**, A44 (2017).
- [65] E. Jullo, S. De La Torre, M.-C. Cousinou, S. Escoffier, C. Giocoli, R. B. Metcalf, J. Comparat, H.-Y. Shan, M. Makler, J.-P. Kneib, et al., *Astronomy & Astrophysics* **627**, A137 (2019).
- [66] H. Gil-Marín, W. J. Percival, L. Verde, J. R. Brownstein, C.-H. Chuang, F.-S. Kitaura, S. A. Rodríguez-Torres, and M. D. Olmstead, *Monthly Notices of the Royal Astronomical Society* p. stw2679 (2016).
- [67] J. Byun, F. O. Franco, C. Howlett, C. Bonvin, and D. Obreschkow, *Monthly Notices of the Royal Astronomical Society* **497**, 1765 (2020).
- [68] L. Perenon, S. Ilić, R. Maartens, and A. de la Cruz-Dombriz, *Astronomy & Astrophysics* **642**, A116 (2020).
- [69] C. Blake and K. Glazebrook, *The Astrophysical Journal* **594**, 665 (2003).
- [70] T. M. C. Abbott, M. Aguena, A. Alarcon, S. Allam, O. Alves, A. Amon, F. Andrade-Oliveira, J. Annis, S. Avila, D. Bacon, et al., *Phys. Rev. D* **105**, 023520 (2022), 2105.13549.
- [71] M. Chevallier and D. Polarski, *International Journal of Modern Physics D* **10**, 213 (2001).
- [72] E. V. Linder, *Physical Review Letters* **90**, 091301 (2003).
- [73] S. Alam, M. Aubert, S. Avila, C. Balland, J. E. Bautista, M. A. Bershad, D. Bizyaev, M. R. Blanton, A. S. Bolton, J. Bovy, et al., *Physical Review D* **103**, 083533 (2021).

- [74] D. J. Bacon, R. A. Battye, P. Bull, S. Camera, P. G. Ferreira, I. Harrison, D. Parkinson, A. Pourtsidou, M. G. Santos, L. Wolz, et al., *Publications of the Astronomical Society of Australia* **37** (2020).
- [75] M. Vargas-Magana, D. D. Brooks, M. M. Levi, and G. G. Tarle, arXiv preprint arXiv:1901.01581 (2019).
- [76] A. Aghamousa, J. Aguilar, S. Ahlen, S. Alam, L. E. Allen, C. A. Prieto, J. Annis, S. Bailey, C. Balland, O. Ballester, et al., arXiv preprint arXiv:1611.00036 (2016).
- [77] S. Ilić, N. Aghanim, C. Baccigalupi, J. R. Bermejo-Climent, G. Fabbian, L. Legrand, D. Paoletti, M. Ballardini, M. Archidiacono, M. Douspis, et al., *Astronomy & Astrophysics* **657**, A91 (2022).
- [78] K. N. Abazajian, K. Arnold, J. Austermann, B. Benson, C. Bischoff, J. Bock, J. Bond, J. Borrill, E. Calabrese, J. Carlstrom, et al., *Astroparticle Physics* **63**, 66 (2015).
- [79] M. Ballardini and R. Maartens, *Monthly Notices of the Royal Astronomical Society* **510**, 4295 (2022).
- [80] E. Castorina, S. Foreman, D. Karagiannis, A. Liu, K. W. Masui, P. D. Meerburg, L. B. Newburgh, P. O'Connor, A. Obuljen, H. Padmanabhan, et al., arXiv preprint arXiv:2002.05072 (2020).
- [81] P. Ade, J. Aguirre, Z. Ahmed, S. Aiola, A. Ali, D. Alonso, M. A. Alvarez, K. Arnold, P. Ashton, J. Austermann, et al., *Journal of Cosmology and Astroparticle Physics* **2019**, 056 (2019), 1808.07445.
- [82] K. N. Abazajian, P. Adshead, Z. Ahmed, S. W. Allen, D. Alonso, K. S. Arnold, C. Baccigalupi, J. G. Bartlett, N. Battaglia, B. A. Benson, et al., arXiv e-prints arXiv:1610.02743 (2016), 1610.02743.
- [83] E. Rath, W. Naidoo, and K. Moodley, *In prep* (2023).
- [84] M. Aich, W. Naidoo, and K. Moodley, *In prep*. (2023).
- [85] Z. Kader and et al., *In prep*. (2023).
- [86] R. Thaman and et al., *In prep*. (2023).